RSC Advances

PAPER

View Article Online
View Journal | View Issue

Cite this: *RSC Adv.*, 2022, **12**, 31729

Hydrothermal synthesis of carbon quantum dots with size tunability *via* heterogeneous nucleation†

Nant Nammahachak,[a] Kamonwan Khamphumee Aup-Ngoen,*[b] Piyapong Asanithi,[c] Mati Horpratum,[d] Surawut Chuangchote,[ae] Sutatch Ratanaphan*[afg] and Werasak Surareungchai[f]

Received 22nd September 2022
Accepted 28th October 2022

DOI: 10.1039/d2ra05989d

rsc.li/rsc-advances

Hydrothermal synthesis has been extensively utilized for fabricating carbon quantum dots (CQDs). Generally, the average sizes of the CQDs are controlled by using specific precursor concentrations, processing temperatures, and reaction times. In our study, the average size of CQDs can simply be controlled by using a different filling volume of sucrose solution in the hydrothermal reactor while keeping the other experimental parameters constant. If homogeneous nucleation plays a major role in the hydrothermal synthesis, the CQDs synthesized by using different filling volumes should have relatively the same size. Nonetheless, we found that the average size of CQDs is inversely correlated with the filling volumes. Particularly, for the hydrothermal syntheses with the filling volumes of 20%, 50%, and 80%, the average size of the CQDs is 15, 13, and 4 nm, respectively. Therefore, the hydrothermal synthesis of CQDs with size-tunability can be achieved by the heterogeneous process associated with the total surface areas between the precursor and reactor.

Introduction

Carbon quantum dots (CQDs) have drawn considerable attention owing to their excellent biocompatibility, chemical inertness, water solubility, and low toxicity.[1–6] There are many synthesis approaches to fabricate CQDs (for example, reduction method,[2] pyrolysis,[7] acidic oxidation,[8] and electrochemical synthesis[9]), but these methods are rather complicated or expensive compared with a hydrothermal synthesis.[1–6] Although carbonization and polymerization play a major role on the average size of CQDs, it is not possible to observe these activities in the black box/hydrothermal reactor.[10–12] In other words, our knowledge on the CQD size distributions was only empirically determined from the experimental inputs of hydrothermal process (*i.e.* concentration of organic precursors, processing temperature, and reaction time).[10–12] As a result, nucleation and growth mechanisms of the CQDs are not well described due to limited configurations of the experimental inputs.

It was reported that the sizes of CQDs derived from the hydrothermal treatment of sucrose precursor were strongly influenced by the decomposition and polymerization.[12] Particularly during the decomposition, sucrose in aqueous solution is hydrolyzed into fructose and glucose, and subsequently decomposed to smaller organic compounds (*i.e.* furfurals and weak acids).[11,12] These organic compounds are then polymerized into larger molecules, which finally lead to the formation of the CQDs in the hydrothermal reactor.[12–14] While homogeneous nucleation is well investigated for metals, ceramics, and organic compounds, its activation free energy is generally larger than a heterogeneous nucleation.[15–18] Considering that the surface of the hydrothermal reactor could provide favorably kinetic pathways for the nucleation of CQDs, the heterogeneous nucleation is expected to be the key mechanism for the nucleation of the CQDs in the hydrothermal reactor. In other words, the classical nucleation theory[19] can be used to evaluate the free energy barriers associated with the formations of critical nuclei for the heterogeneous nucleation. It is known that existences of foreign substances (*i.e.* reactor wall, impurities, and foreign particle) can significantly reduce the energy barriers for nucleation.[15–17]

[a]*Department of Tool and Materials Engineering, King Mongkut's University of Technology Thonburi, 126 Prachauthit Road, Bangmod, Bangkok 10140, Thailand. E-mail: sutatch.ratanaphan@mail.kmutt.ac.th*

[b]*Materials and Nondestructive Testing Laboratory, King Mongkut's University of Technology Thonburi (KMUTT, Ratchaburi), 126 Pracha Uthit Rd, Thung Khru, Bangkok 10140, Thailand. E-mail: kamonwan.aup@kmutt.ac.th*

[c]*Department of Physics, Faculty of Science, King Mongkut's University of Technology Thonburi, 126 Prachauthit Road, Bangmod, Bangkok 10140, Thailand*

[d]*Opto-Electrochemical Sensing Research Team (OEC), National Electronic and Computer Technology Center, 112 Thailand Science Park, Pahonyothin Rd, Khlong Nueng, Khlong Luang, Pathum Thani 12120, Thailand*

[e]*Research Center of Advanced Materials for Energy and Environmental Technology (MEET), King Mongkut's University of Technology Thonburi, 126 Prachauthit Road, Bangmod, Bangkok 10140, Thailand*

[f]*Nanoscience and Nanotechnology Graduate Program, King Mongkut's University of Technology Thonburi, 126 Prachauthit Road, Bangmod, Bangkok 10140, Thailand*

[g]*Center of Excellence in Theoretical and Computational Science Center (TaCS-CoE), King Mongkut's University of Technology Thonburi, 126 Pracha Uthit Rd, Thung Khru, Bangkok 10140, Thailand*

† Electronic supplementary information (ESI) available. See DOI: https://doi.org/10.1039/d2ra05989d

As a result, nuclei nucleated heterogeneously on the reactor wall is more frequently occurred comparing with the one nucleated inside the liquid precursor and the number of heterogeneous nuclei are linearly proportional to the total surface area of the reactor.[15,20] In order to study the heterogeneous nucleation in the hydrothermal CQDs, different filling volumes of sucrose solution in the hydrothermal reactor are used while keeping the other experimental parameters constant (such as, reactor geometry, concentration of the precursor, processing temperature, and reaction time). Analyses of the sizes of CQDs and activation free energies for homogeneous and heterogeneous nucleation are also discussed by using the classical nucleation theory.

Experimental section

Sucrose [purity ≥99.5%, Sigma Aldrich] dissolved in deionized water (DI) with 2 wt% has been used for all hydrothermal syntheses of the CQDs. To investigate the influence of precursor filling volumes on the size distributions of CQDs, the precursor was placed into a Teflon lined stainless steel autoclave (diameter = 50 mm, height = 100 mm, and volume = 200 ml) with a different filling volume (20%, 50%, and 80% of the total capacity). The hydrothermal reactor was then annealed in a hot air furnace (Binder) at 180 °C for 2 hours and gradually cooled to a room temperature. Morphology and particle size of CQDs were determined using a high-resolution transmission electron microscope (HRTEM; FEI Tecnai G2 20). Chemical bonding and surface functional groups of the CQDs were characterized using Fourier transform infrared spectroscopy (FTIR, Thermo scientific) with wavenumbers ranging from 800 cm^{-1} to 3600 cm^{-1}. Raman (Renishaw) spectroscopy with an excitation wavelength of 532 nm was used to characterize the graphitic level of the CQDs. Fluorescence properties of the CQDs were obtained by using a Tecan Infinite M200 spectrophotometer and the quantum yields (QYs) of CQDs were determined by using quinine sulfate as a reference.

Results and discussion

The hydrothermal syntheses of the CQDs with different filling volumes lead to distinct size distributions as shown in TEM images (Fig. 1). Specifically, the average sizes of CQDs increased from 4 ± 1 nm to 13 ± 1.6 nm and 15 ± 1.4 nm when the filling volumes of 80% to 50% and 20% are used, respectively. All experiments are repeated three times with comparable size distributions (Fig. S1, ESI†). While average sizes of the CQDs are inversely correlated with the filling volumes of the sucrose precursor solutions in the hydrothermal reactor (Table S1, ESI†), the size distributions of these CQDs are well described by a normal distribution (Fig. 1a–c). Therefore, growth mechanism of the CQDs, which are composed of well-ordered graphite (002) plane with an interplanar spacing of 0.36 nm[10,12] as shown in a HRTEM image (Fig. 1d), are comparable regardless of the filling volumes. The chemical analyses of the CQDs using FTIR and Raman spectroscopies in Fig. 2 clearly demonstrated that the surface functional group of these CQDs are mainly

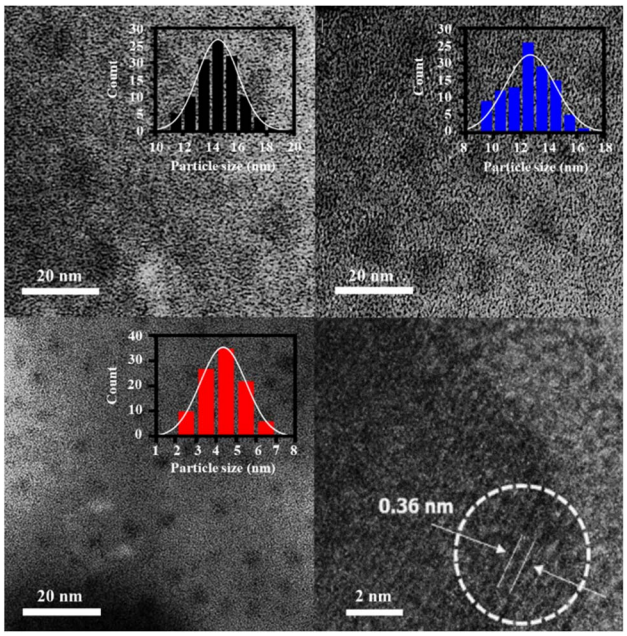

Fig. 1 TEM images of the CQDs prepared with the filling volumes of 20% (a), 50% (b), and 80% (c). The insets show the size distributions of the CQDs synthesized using 20% (15 ± 1.4 nm), 50% (13 ± 1.6 nm), and 80% (4 ± 1 nm). High-resolution TEM image of the CQDs prepared with the filling volume of 80% demonstrates an interplanar spacing of 0.36 nm (d).

composed of oxygen containing groups (*i.e.* hydroxyl, carboxylic, and carbonyl), consistent with the previous studies that used glucose as precursors for the hydrothermal synthesis of CQDs.[10,12] While the surface functional groups of the CQDs are relatively comparable regardless of their sizes, the intensity ratios between the D and G bands (I_D/I_G) in Table S1, ESI† indicates that the disorder structures are increased during the growth of the CQDs.[11,12,14]

A change in the color from dark to light brown is observed in the hydrothermal solutions synthesized with the filling volumes from 20% to 80% under the ambient light (Fig. S2a, ESI†), however, these solutions containing the CQDs show only green fluorescence under ultraviolet lamp (415 nm). The fluorescent emission spectra of these CQDs show excitation-dependent emission, consistent with the previous studies.[11,12,21] Particularly, the peak intensities centered on around 450 nm corresponded to an excitation wavelength of 360 nm (90 nm Stokes shift) are observed in the CQDs specimens regardless of their sizes (Fig. S2b–d, ESI†)). If the QYs is only correlated with the I_D/I_G, the CQDs with average sizes of 4 nm should have the largest QYs. Nonetheless, the QYs of the CQDs with average sizes of 4 nm (I_D/I_G = 0.63) and 13 nm (I_D/I_G = 0.67) are relatively comparable (Table S1, ESI†). Therefore, the fluorescent emission intensities of the CQDs were contributed from the interaction between the sp^2 graphite structure and their surrounding media,[11,22] resulting in the differences in the QYs of the CQDs with equivalent chemical basis (Table S1, ESI†).

While classical nucleation theory has been used to describe the formation of nanostructures in various materials (metals,

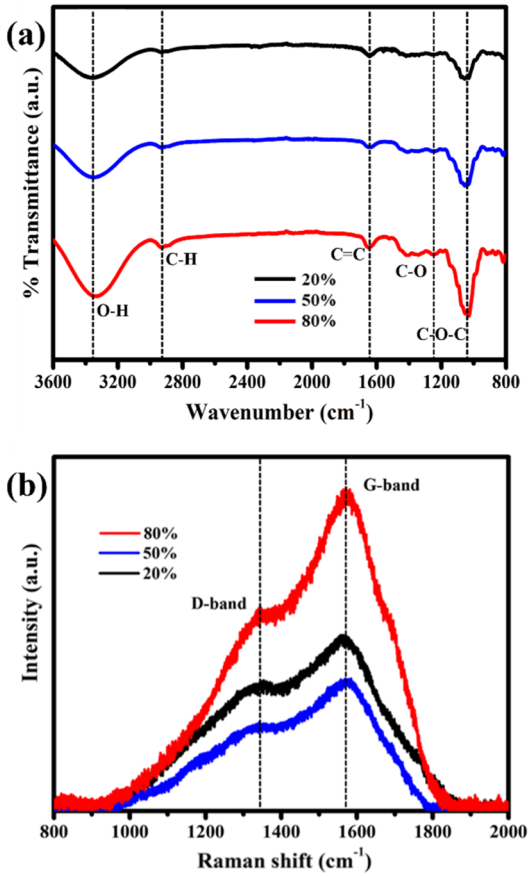

Fig. 2 FTIR (a) and Raman spectra (b) of the CQDs synthesized by using the filling volumes of 20% (black), 50% (blue), and 80% (red).

ceramics, organic, and inorganic compounds),[15–17,23] it was never applied to describe the heterogeneous nucleation in the hydrothermal CQDs. Because the transformations of one-dimensional carbon chains to graphene, two-dimensional graphene, and finally to three-dimensional CQDs are rather complicated and could be strongly influenced by the derivative organic compounds of sucrose.[12,24] Ones would doubt the applicability of classical nucleation theory to quantify the nucleation mechanisms in the hydrothermal reactor. However, previous studies demonstrated that homogeneous and heterogeneous nucleation of organic compounds (such as, glycine, amyloid beta, and isonicotinamide) can be well described by the classical nucleation theory.[15,25,26] If homogeneous nucleation plays a major role on the nucleation and growth in the hydrothermal synthesis, the CQDs synthesized by using different filling volumes should have comparable size distributions. In addition, if the rates of heterogeneous nucleation are continuous during hydrothermal synthesis, the size distribution of CQDs is expected to be a broad distribution. Nonetheless, the size distributions of CQDs prepared with the different filling volumes are not only different but also have narrow distributions as shown in Fig. 1, suggesting that heterogeneous nucleation is a primary mechanism for the formation of the CQDs. According to the classical nucleation theory,[19] the total free energy of homogeneous nucleation of the CQDs with spherical nucleus (ΔG_{homo}) as a function of its radius (r) is given by

$$\Delta G_{homo} = 4/3\pi r^3 \Delta G_{\upsilon} + 4\pi r^2 \gamma_{gw} \quad (1)$$

where ΔG_{υ} is the free energy difference per unit volume between the initial and final phases associated with the nucleation. Due to the complexity of the chemical reactions during the phase transformation, it is literally not possible to consider all of the chemical components related to the nucleation processes. We assume that the ΔG_{υ} is approximately equal to the changes in the free energy per unit volume for the formation of graphene (4.59×10^8 J m^{-3}).[27] While the solute concentrations of the surrounding media could influence to an interfacial energy between the nucleus and surrounding as observed for glycine, $CaCO_3$, and silica,[15,16,23] the concentrations of the precursor residues and their derivatives obtained from the hydrothermal solution of only 2 wt% sucrose are expected to be less influenced to the interfacial energy. In this case, γ_{gw} is approximated by the interfacial energy measured between graphene and DI water (83 mJ m^{-2}).[28] Because the activation energy for the heterogeneous nucleation (4.54×10^{-20} J), ($\Delta G^*_{hetero} = f(\theta)\Delta G^*_{homo}$), is lower than for the homogeneous nucleation (4.12×10^{-20} J), the overall rate of the CQD nucleation is contributed from the heterogeneous nucleation as shown in Fig. 3a. Note that for the CQDs, the contact angle ($\theta = 128.7°$) is determined from the Young equation.[17]

$$\gamma_{tw} = \gamma_{gt} + \gamma_{gw}\cos\theta \quad (2)$$

where the surface energies between Teflon–DI water (γ_{tw}) and graphene–Teflon (γ_{gt}) are equal to 27 mJ m^{-2} (ref. 29) and 79 mJ m^{-2}, respectively. Due to the difference in the activation energy associated with $f(\theta) = \frac{1}{4}(2 - 3\cos\theta + \cos\theta^3) = 0.91$, it is expected that the smaller organic compounds obtained from a dehydration of sucrose during the heating[12,30] are preferably polymerized into larger molecules and finally carbonized into the CQDs on the reactor wall during the cooling period (an inset in Fig. 3a). Assuming that the precursor solutions and the reactor wall are in thermal equilibrium after 2 hours annealing at 180 °C in a hot air furnace, the temperature gradient is expected to promote large amount of the heterogeneous nucleation during the cooling period, resulting in the narrow distributions of CQDs. The fluid flows induced from the temperature gradients[20] during the cooling might also enhance the mixing of the heterogeneous nuclei with the derivative precursors in the hydrothermal reactor. Fig. 3b shows the relationships between the filling volumes and the average sizes of the CQDs, graphene hydroxyapatite (GHA), zinc ferrite ($ZnFe_2O_4$), and titanium dioxide (TiO_2). Interestingly, the average size of the CQDs, GHA, and $ZnFe_2O_4$ are all inversely correlated with the precursor filling volumes.[31,32] Nonetheless, the sizes of TiO_2 are not depended on the filling volumes.[33] Although the activation energy for heterogeneous nucleation is also lower than the homogeneous nucleation for TiO_2, it should be noted that the energy difference in TiO_2 (1.55×10^{-21} J) calculated from TiO_2–Teflon ($\gamma_{TiO_2t} = 57$ mJ m^{-2}) and TiO_2–DI water ($\gamma_{TiO_2w} = 72$ mJ

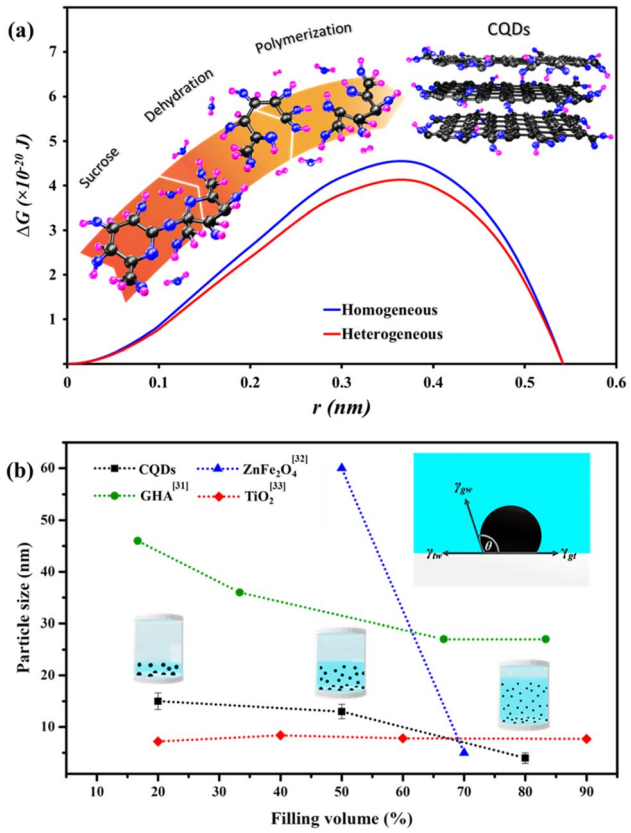

Fig. 3 Comparison between activation energies for homogeneous and heterogeneous nucleation of the CQDs (a). The inset in (a) shows formation mechanism of the CQDs composed of two major steps, dehydration of sucrose and polymerization of smaller compounds. Relationship between the filling volumes of hydrothermal precursors and the average sizes of CQDs (b). The heterogeneous nucleation of a CQD on the Teflon surface shows as an inset in (b). The previous results for graphene hydroxyapatite (GHA), zinc ferrite ($ZnFe_2O_4$), and titanium dioxide (TiO_2)[31–33] are also included in the plot. Surface energies, Teflon–DI water (γ_{tw}), graphene–Teflon (γ_{gt}), and graphene–DI water (γ_{gw}) are obtained from ref. 28 and 29.

m^{-2})[34] is significantly lower than the one in the CQD (4.08×10^{-21} J). Considering that the magnitude of energy difference in TiO_2 is comparable with the thermal energy ($k_BT = 6.25 \times 10^{-21}$ J), it is expected that the rates of homogeneous nucleation and heterogeneous nucleation are negligible different, resulting in the average sizes that are not inversely correlated with the filling volumes.

Conclusions

In summary, hydrothermal carbon quantum dots (CQDs) with average sizes ranging from 4 to 15 nm have been simply obtained by hydrothermal syntheses with different filling volumes of sucrose solution in the hydrothermal reactor. Because the CQDs are synthesized with the same sucrose concentration, hydrothermal autoclave, and temperature profile, the differences in the CQD sizes are strongly influenced by the filling volumes or the heterogeneous surface between the precursor and reactor. In this respect, experimental parameters for a large-scale fabrication of the CQDs should not only be considered the precursor concentrations, processing temperatures, and reaction times, but also included the heterogeneous interfaces.

Conflicts of interest

There are no conflicts to declare.

Acknowledgements

We gratefully acknowledge the financial supports from the Petchra Pra Jom Klao PhD Research Scholarship from King Mongkut's University of Technology Thonburi, the Thailand Science Research and Innovation (TSRI) under Fundamental Fund (Project: Advanced Materials and Manufacturing for Applications in New S-curve Industries) and the Development and Promotion of Science and Technology Talents Project (DPST).

Notes and references

1 C. Wang, Z. Xu, H. Cheng, H. Lin, M. G. Humphrey and C. Zhang, *Carbon*, 2015, **82**, 87–95.
2 K. Linehan and H. Doyle, *J. Mater. Chem. C*, 2014, **2**, 6025–6031.
3 Y. Guo, Z. Wang, H. Shao and X. Jiang, *Carbon*, 2013, **52**, 583–589.
4 Z. X. Liu, Z. L. Wu, M. X. Gao, H. Liu and C. Z. Huang, *Chem. Commun.*, 2016, **52**, 2063–2066.
5 S. Liu, Y. He, Y. Liu, S. Wang, Y. Jian, B. Li and C. Xu, *Chem. Commun.*, 2021, **57**, 3680–3683.
6 W. He, W. Weng, X. Sun, Y. Pan, X. Chen, B. Liu and J. Shen, *ACS Appl. Nano Mater.*, 2020, **3**, 7420–7427.
7 M. C. Ortega-Liebana, N. X. Chung, R. Limpens, L. Gomez, J. L. Hueso, J. Santamaria and T. Gregorkiewicz, *Carbon*, 2017, **117**, 437–446.
8 X. Wang, L. Cao, F. Lu, M. J. Meziani, H. Li, G. Qi, B. Zhou, B. A. Harruff, F. Kermarrec and Y.-P. Sun, *Chem. Commun.*, 2009, 3774–3776.
9 Q.-L. Zhao, Z.-L. Zhang, B.-H. Huang, J. Peng, M. Zhang and D.-W. Pang, *Chem. Commun.*, 2008, 5116–5118.
10 Z.-C. Yang, M. Wang, A. M. Yong, S. Y. Wong, X.-H. Zhang, H. Tan, A. Y. Chang, X. Li and J. Wang, *Chem. Commun.*, 2011, **47**, 11615–11617.
11 L. Tang, R. Ji, X. Li, K. S. Teng and S. P. Lau, *Part. Part. Syst. Charact.*, 2013, **30**, 523–531.
12 H. K. Sadhanala, J. Khatei and K. K. Nanda, *RSC Adv.*, 2014, **4**, 11481–11485.
13 M. L. Liu, B. B. Chen, C. M. Li and C. Z. Huang, *Green Chem.*, 2019, **21**, 449–471.
14 G. Liu, S. Li, M. Cheng, L. Zhao, B. Zhang, Y. Gao, Y. Xu, F. Liu and G. Lu, *New J. Chem.*, 2018, **42**, 13147–13156.
15 Y. Kamano, K. Kadota, A. Shimosaka, Y. Shirakawa and J. Hidaka, *J. Mol. Liq.*, 2014, **200**, 474–479.
16 L. M. Hamm, A. J. Giuffre, N. Han, J. Tao, D. Wang, J. J. D. Yoreo and P. M. Dove, *Proc. Natl. Acad. Sci. U. S. A.*, 2014, **111**, 1304–1309.

17 J. Zhao, M. Wang, H. M. S. Lababidi, H. Al-Adwani and K. K. Gleason, *Desalination*, 2018, **442**, 75–88.
18 A. Yoko, S. Okabe, G. Seong, T. Tomai and T. Adschiri, *J. Supercrit. Fluids*, 2020, **159**, 104749.
19 K. Kelton and A. L. Greer, *Nucleation in Condensed Matter: Applications in Materials and Biology*, Elsevier, 2010.
20 Z.-Y. Ma, Z.-L. Yu, Z.-L. Xu, L.-F. Bu, H.-R. Liu, Y.-B. Zhu, B. Qin, T. Ma, H.-J. Zhan, L. Xu, H.-A. Wu, H. Ding and S.-H. Yu, *Matter*, 2020, **2**, 1270–1282.
21 P. Suvarnaphaet, C. S. Tiwary, J. Wetcharungsri, S. Porntheeraphat, R. Hoonsawat, P. M. Ajayan, I.-M. Tang and P. Asanithi, *Mater. Sci. Eng., C*, 2016, **69**, 914–921.
22 Z.-H. Wen and X.-B. Yin, *RSC Adv.*, 2016, **6**, 27829–27835.
23 D. Gebauer, M. Kellermeier, J. D. Gale, L. Bergström and H. Cölfen, *Chem. Soc. Rev.*, 2014, **43**, 2348–2371.
24 J. Gao, J. Yip, J. Zhao, B. I. Yakobson and F. Ding, *J. Am. Chem. Soc.*, 2011, **133**, 5009–5015.
25 A. K. Srivastava, J. M. Pittman, J. Zerweck, B. S. Venkata, P. C. Moore, J. R. Sachleben and S. C. Meredith, *Protein Sci.*, 2019, **28**, 1567–1581.
26 S. A. Kulkarni, S. S. Kadam, H. Meekes, A. I. Stankiewicz and J. H. ter Horst, *Cryst. Growth Des.*, 2013, **13**, 2435–2440.
27 J. Yang, X. Li, S. Han, R. Yang, P. Min and Z.-Z. Yu, *J. Mater. Chem. A*, 2018, **6**, 5880–5886.
28 C. D. van Engers, N. E. A. Cousens, V. Babenko, J. Britton, B. Zappone, N. Grobert and S. Perkin, *Nano Lett.*, 2017, **17**, 3815–3821.
29 D. Mańko, A. Zdziennicka and B. Jańczuk, *Appl. Surf. Sci.*, 2017, **392**, 117–125.
30 M. O. Dekaliuk, O. Viagin, Y. V. Malyukin and A. P. Demchenko, *Phys. Chem. Chem. Phys.*, 2014, **16**, 16075–16084.
31 H. Nosrati, R. S. Mamoory, F. Dabir, D. Q. Svend Le, C. E. Bünger, M. C. Perez and M. A. Rodriguez, *Ceram. Int.*, 2019, **45**, 1761–1769.
32 P. S. Yoo, B. W. Lee and C. Liu, *IEEE Trans. Magn.*, 2015, **51**, 1–4.
33 A. H. Mamaghani, F. Haghighat and C.-S. Lee, *J. Photochem. Photobiol., A*, 2019, **378**, 156–170.
34 A. Saptoro, Y. Kanazawa, M. Asada, Y. Asakuma and C. Phan, *Exp. Therm. Fluid Sci.*, 2016, **72**, 228–234.